Showcasing research from Professor Huang Zhang's laboratory, School of Electrical and Electronic Engineering, Harbin University of Science and Technology, China.

Prospects of single atom catalysts for dendrite-free alkali metal batteries

The review of single-atom catalyst (SAC) technology for the manipulation of alkaline metal anodes in batteries has highlighted the efficient role in manipulating the alkali metal anode in batteries. Sustainable paths for future critical battery chemistry and material selections based on SACs are further prospected to achieve advanced and sustainable alkali metal batteries.

As featured in:

See Jian Wang, Huang Zhang, Hongzhen Lin *et al.*, *Green Chem.*, 2024, **26**, 10366.

ROYAL SOCIETY OF CHEMISTRY

rsc.li/greenchem

Registered charity number: 207890

Green Chemistry

ROYAL SOCIETY OF CHEMISTRY

CRITICAL REVIEW

View Article Online
View Journal | View Issue

Cite this: *Green Chem.*, 2024, **26**, 10366

Prospects of single atom catalysts for dendrite-free alkali metal batteries

Huihua Li,[a] Jian Wang, *[b,c,e] Jing Zhang,[d] Lujie Jia,[b] Hongxu Qu,[a] Qinghua Guan,[b] Huang Zhang *[a] and Hongzhen Lin*[b]

High-energy-density alkali metal batteries (AMBs) offer a potentially promising and sustainable option for energy storage. However, notorious dendrite growth and uncontrollable plating behaviors resulting from random spatial ion/atom distribution and related high barriers restrict the development of AMBs. Different from interphase engineering and architecture construction, the emerging catalysis modulation is proposed to overcome above-related barriers, achieving uniform alkali metal nucleation and atom diffusion. Among the various catalysts, single atom catalysts (SACs) exhibit an atomic exposure of nearly 100%, displaying high atomic catalytic capability and efficiency. Although it is still at an early stage, the adoption of SACs for modulating alkali metal ion/atom desolvation or diffusion has shown great promise in both fundamental research and practical applications. In this review, the fabrications and characterizations of SACs are briefly summarized, and the principal mechanisms of SAC-incorporated alkali metal anode systems are highlighted in terms of electrochemical analysis, microscopic/spectroscopic characterizations, and theoretical simulations. In addition, sustainable paths for future critical battery chemistry and material selections based on SACs are highlighted. The associated opportunities and challenges are further prospected to achieve a high-performance alkali metal anode.

Received 28th May 2024,
Accepted 18th July 2024

DOI: 10.1039/d4gc02590c

rsc.li/greenchem

[a]*School of Electrical and Electronic Engineering, Harbin University of Science and Technology, Harbin 150080, P. R. China. E-mail: zhang.huang@hrbust.edu.cn*
[b]*i-Lab, Suzhou Institute of Nano-Tech and Nano-Bionics, Chinese Academy of Sciences, Suzhou 215123, China. E-mail: hzlin2010@sinano.ac.cn*
[c]*Helmholtz Institute Ulm (HIU), Ulm 89081, Germany. E-mail: jian.wang@kit.edu*
[d]*School of Materials Science and Engineering, Xi'an University of Technology, Xi'an 710048, China*
[e]*Karlsruhe Institute of Technology (KIT), Karlsruhe D-76021, Germany*

1. Introduction

In the pursuit of a sustainable future, the significance of renewable energy sources and energy storage solutions is growing ever more pivotal. Rechargeable lithium ion batteries (LIBs) have become indispensable in our daily smart life owing to their high energy densities and portability.[1] However, to reach the expected energy density of 500 W h kg^{-1} for electric

Huihua Li

Huihua Li is currently Associate Professor at the Harbin University of Science and Technology. She received her Ph.D. in physical chemistry from Karlsruhe Institute of Technology in 2022. Afterward, she worked as a post-doctor at Helmholtz Institute Ulm. Her research interests are focused on electrolyte and electrode materials for rechargeable sodium batteries.

Jian Wang

Jian Wang is a research fellow supported by the Alexander von Humboldt Foundation at Helmholtz Institute Ulm (HIU), Karlsruhe Institute of Technology (KIT) after receiving a PhD degree from the University of Science and Technology of China (USTC). His research interests focus on the construction of catalysis in secondary batteries ("Catalysis-in-Batteries") and the exploration of in situ/operando *characterizations for probing catalytic mechanisms.*

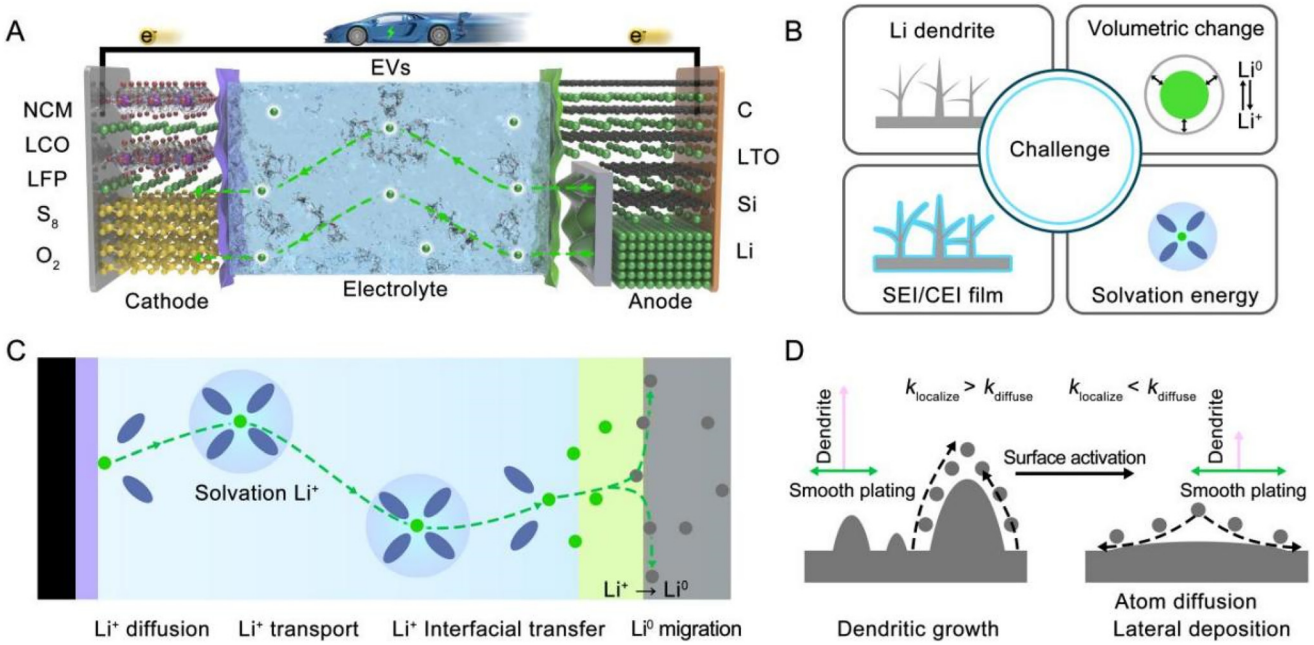

Fig. 1 (A) Schematic of LMBs and (B) the corresponding challenges. (C) Systematic scheme of Li behaviors from the electrolyte to the electrode. (D) The competing kinetics between Li^0 localization with dendrite growth and Li^0 diffusion with lateral deposition.

vehicles (EVs), conventional LIBs have encountered capacity bottlenecks owing to the limited specific capacities of cathodes and graphite anodes.[2–4] Alternatively, alkali metal anodes exhibit amazing superiorities such as the lowest standard potential and high specific capacity, thus resulting in high energy density. For example, a Li metal electrode shows a capacity of 3860 mA h g^{-1}, which is about ten times higher than that of a commercial graphite anode (Fig. 1A).[5–8] However, several challenges still remain that inhibit the development of alkali metal batteries (AMBs):[9–20] (1) the dendrite growth resulting from uncontrollable deposition behaviors, causing severe safety problems; (2) the pulverization and formation of "dead Li/Na"; (3) the repeated disruption and formation of a solid-electrolyte interphase (SEI) on a metal surface. These problems are never independent but are complicated *via* intrinsic interactions (Fig. 1B), especially under harsh conditions such as low-temperatures.[21]

To obtain dendrite-free alkali metal anodes, diverse efforts and strategies have been undertaken to achieve dendrite-free alkali metal anodes with long lifespans: (1) regulating electrolyte components or additives for *in situ* electrochemical generations of a robust SEI;[22–25] (2) employing inorganic/organic artificial function layers with improved mechanical properties on alkali metal surfaces;[26,27] (3) constructing three-dimensional architectures for infusing metallic Li/Na or buffering volumetric expansion;[28–30] (4) constructing conductive carbon or alloy layers to modulate Li^+/neutral lithium atom (Li^0) transport.[16,31–33] As observed, state-of-the-art SEI and host

Huang Zhang

Huang Zhang is Professor at the Harbin University of Science and Technology, and he was formerly Associate Professor at Northwestern Polytechnical University. He has been a predoctoral research fellow at KU Leuven. Afterward, he received his PhD from Karlsruhe Institute of Technology and worked as a junior scientist at Helmholtz Institute Ulm. His research interests focus on the basic understanding and development of materials for advanced and sustainable batteries.

Hongzhen Lin

Hongzhen Lin is a senior researcher at the i-*lab of Suzhou Institute of Nano-Tech and Nano-bionics, Chinese Academy of Sciences and University of Science and Technology of China. He majors in developing high energy density lithium metal-based energy storage systems with catalytic functionalities and their* in situ *interfacial nonlinear spectroscopy characterization.*

design approaches remain hot spots.[12] To the best of our knowledge, taking Li as a representative of alkali metals, the Li plating process consists of several essential steps: interfacial Li^+ desolvation, Li^+ diffusion and interfacial transfer, electroreduction of Li^+ to Li^0, migration and redistribution of Li^0, nucleation and growth, as displayed in Fig. 1C.[3,33,34] These steps are kinetically and/or thermodynamically controlled and are often associated with various competitive processes at the interface. As is known, the positive alkali ionic diffusion behavior is governed by the strength of the electric field, interfacial desolvation, and surface affinity. Fundamentally, as depicted in Fig. 1D, alkali metal dendrite growth, such as Li anode, is attributed to the heterogeneous spatial distribution of formed metal atoms and their sluggish diffusion/migration to separate nucleus sites of metal atoms on the surface, leading to the uncontrollable plating morphologies.[7] Unlike the diffusion behaviors of metal ions, the metal atom diffusion is less sensitive to the electric field and only relies on the interfacial activity. Similarly, delocalizing and spreading metal atoms rapidly across the surface is beneficial for preventing the local metal aggregation and suppressing dendrite growth.[6,7,35–37] Therefore, tuning surface chemistry for rapid diffusion of alkali atoms is essential to achieve uniform and lateral deposition, and the key issue is to clarify the main obstacles to the diffusion barriers of surface atoms and how to minimize them.[3]

To date, single atom catalysts (SACs) with nearly 100% atomic utilization, anchored in nanocarbon or defect-abundant particles, have been deemed the "holy grail" in catalytic fields, opening up a new pathway for catalyzing chemical reactions.[2,8,38–41] Interestingly, SACs have also shown the potential to address the challenges on alkali metal anodes, consequently improving the performance of batteries. In these battery systems, SACs are exposed and endowed with the ability to accelerate solid phase conversions and activate the surface for rapid ion transfer.[40,41] Extending these knowledges into alkali anode studies, SACs have also shown the merits in regulating the ion/atom diffusion and plating behaviors.[8,34,42] In this critical review, the typical synthesis and characterizations of SACs are initially introduced based on initial application in sulfur cathodes; followingly, the studies of SACs for achieving dendrite-free Li/Na/K anodes are reviewed, and the roles of SACs in decreasing the energy barriers of the related chemical processes are surveyed from a generalizable viewpoint from desolvation, diffusion and nucleation; and finally, the sustainable paths for future critical battery chemistry with a special emphasis on materials selections and practical challenges in exploiting SACs for high-performance AMBs are further outlooked.

2. Basic understanding of the synthesis and characterization of SACs

To achieve the modulation effect of SACs in alkali metal anodes, the precise fabrications of stable SACs face severe challenges because they tend to aggregate and grow into nanoclusters or nanoparticles, which greatly lowers the surface energy and reduces the activity.[43–49] Among the reports, the widely used strategy can be classified into two aspects: (1) heteroatom-assisted anchored coordination, typically for N-doping; (2) semiconductor nanocrystals with defect-rich sites as "trapping" sites to stabilize metal atoms.

Wet impregnation and high-temperature pyrolysis of various metal-based precursors are often adopted. The metal ion precursors are preferentially adsorbed on the heteroatom-doped sites *via* sufficient immersion and are then transformed into single metal atoms upon thermal treatment in a specific atmosphere. As shown in Fig. 2A, by dispersing the iron precursor and heteroatom-doped carbon matrix into the anhydrous ethanol suspension, a uniform distribution of single Fe atom catalyst (SAFe) can be achieved in the hybrid composites after evaporation and reduction treatment.[40] Although the wet impregnation method enables simple steps and low cost, the low atom loading concentration and partial agglomeration often limit its wide applications because the atomic concentration is determined by the doping amount of N atoms in nanocarbons.[39,49] Therefore, the strategy of high-temperature pyrolysis is developed, and the SAC precursors are initially coordinated and dispersed by the N-provider. After pyrolysis, single metal atoms are *in situ* anchored onto the carbonized supports. For example, the Co precursors are well embraced by the N-containing polymer after sufficiently mixing, significantly improving the loading concentration of SACs in the nanocomposites (Fig. 2B).[41] After high-temperature treatment, the N-provider is converted into N-doped nanocarbon and serves as the holder to anchor well-distributed Co atoms.

Owing to the unstable chemical environment of defects in metal compounds, the deficient sites are driven to trap metal atoms to fill in the surroundings with high electronic density and low coordinate numbers.[8,50] For instance, with the aid of the atomic layer deposition (ALD) technique, the atomic Au is well-captured by the oxygen vacancy in the TiO_2 and forms a Ti–Au–Ti bonding structure.[51] Because the application of ALD is limited by the expensive facility cost and the complex production process, more feasible methods, such as hydrothermal reactions, are also developed in this regard. As displayed in Fig. 2C, the defect-abundant $Fe_{1-x}S$ was synthesized through the hydrothermal reaction with the reductive atmosphere, acting as a host for locating the single Co atoms simultaneously.[8]

To verify the presence of atomic metal catalysts, aberration-corrected scanning transmission electron microscope (AC-STEM) and X-ray absorption spectroscopy (XAS) are usually combined to observe electronic surroundings and chemical information.[48,52] The bright atoms can be well judged by the difference from the carbon matrix in the high-resolution STEM (Fig. 2D).[8] Apart from observing the concrete morphology of individual atoms, the valence state information of the single atoms can be further obtained by resorting to the corresponding electronic energy loss spectroscopy (EELS) pattern. In the XAS, the near-edge information of the metal atom is available to detect an electronic structure that differs from the references. The Fourier transform is also used to assign the

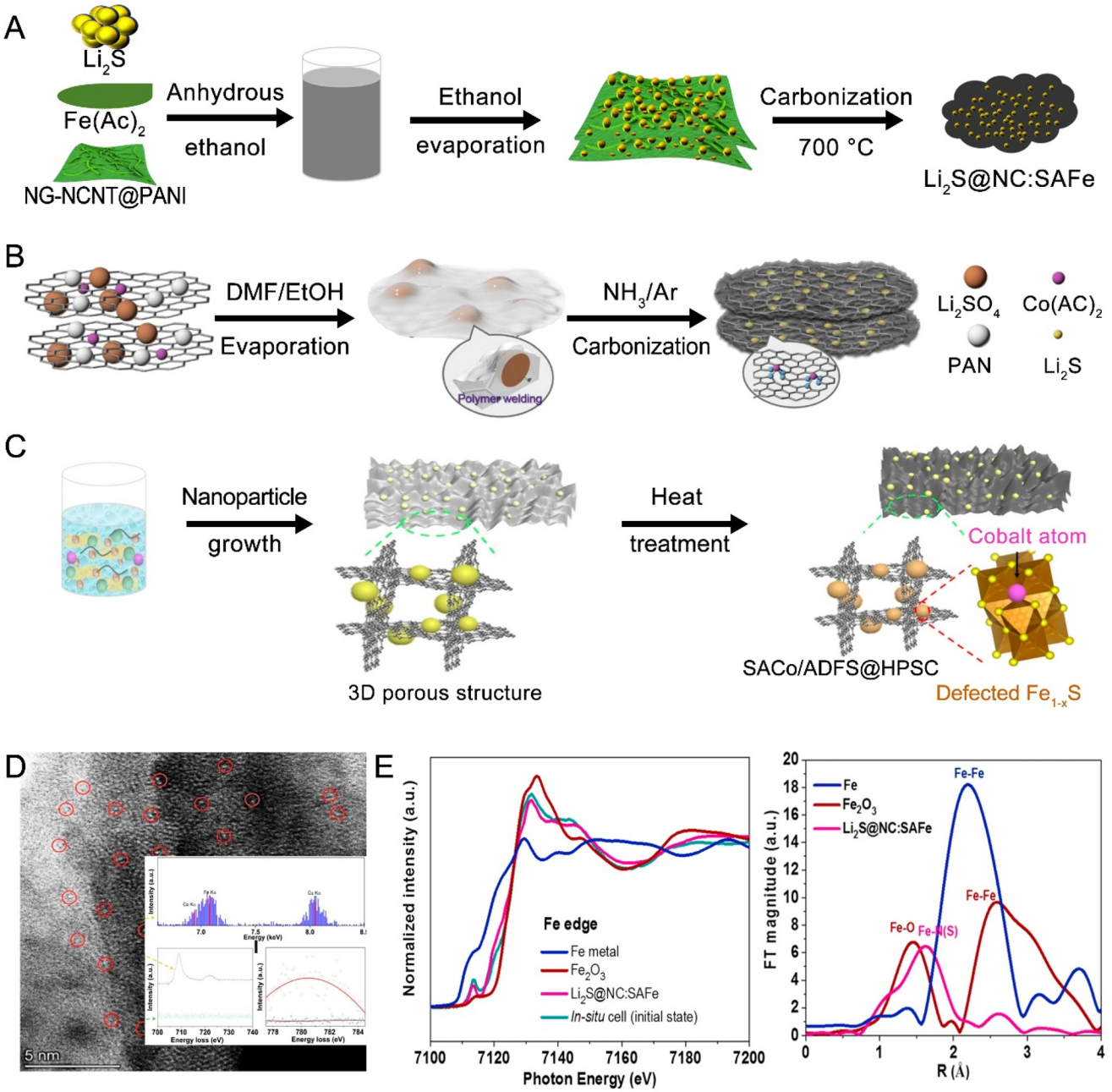

Fig. 2 Synthesis of SACs using a heteroatom-assisted anchored coordination strategy: (A) wet impregnation. Reproduced with the permission.[40] Copyright 2019, Elsevier. (B) High-temperature pyrolysis. Reproduced with permission.[41] Copyright 2020, Elsevier. (C) Defect site-assisted stabilization. The atomic characterizations of SACs through (D) AC-STEM with EELS. Reproduced with permission.[8] Copyright 2021, American Chemical Society. (E) XAS. Reproduced with permission.[40] Copyright 2019, Elsevier.

coordination number and coordinate the bond between the central atoms and neighboring atoms (Fig. 2E).[40]

3. Roles of SACs in high-performance Li metal batteries

In Li metal batteries, the utilization of Li metal anodes during plating/stripping remains one of the most practical challenges to overcome. From the aspect of architecture design, the Li^+ diffusion in electrolyte and across SEI/cathode-electrolyte interphase (CEI) and electrode materials has been extensively studied, and various strategies for constructing artificial layers or hosts have been reported to enable the efficient operation of Li metal anodes. However, poor knowledge of dynamic kinetics makes it hard to effectively reduce the barriers of Li^+ desolvation, diffusion, and nucleation at the interface, which are responsible for sluggish kinetics.[53] As discussed above, the

constructions of 3D current collectors with lithiophilic sites effectively reduce the local current density and promote uniform nucleation of Li^+. Unfortunately, the electron-coupled Li atom (Li^0) is non-sensitive to the electric field, usually relaxes quickly and localizes in a confined region with limited diffusion owing to the higher diffusion barrier. In this case, the Li dendrites are also formed during the long-term plating/stripping process. Meanwhile, the large applications of 3D current collectors sacrifice the energy density of Li anodes. Therefore, how to effectively manipulate the Li behaviors across the interface and diffuse around the Li surface is much more important. By bringing the metal-based or alloy modulators down to the atomic level, the energy barriers of Li^+ deposition at the interface can be reduced, and the Li^0 diffusion path can be optimized. In this section, the behaviors of Li desolvation, nucleation, and diffusion are discussed in detail under the modulation of SAC.

3.1 SAC in facilitating interfacial Li^+-solvent desolvation

As known, the dissociation degree of the Li^+ solvation shell at the interface during electroplating is related to the subsequent Li^+ migration across the interface and further uniform Li^0 diffusion.[3,54] The desolvation of solvated Li^+ has a high energy barrier, which is the decisive step in the process of Li^+ migration and Li^0 diffusion candidates during plating.[50,55,56] To deal with the desolvation barrier, our previous work first demonstrated the electrocatalytic method to dissociate Li^+ from Li^+-solvent molecular clusters.[50] Fe-based atomic catalysts were developed as compelling candidates due to their intrinsic sustainability and practical applicability. Briefly, atomic Fe was anchored on cation vacancy-rich $Co_{1-x}S$ embedded in 3D porous carbon (SAFe/CVRCS@3DPC), as demonstrated by theoretical simulation with the lowest formation energy, acting as an interfacial promoter. Furthermore, the solvation structures of Li^+ with different degrees of coordination were intimated. As the coordination number increases around Li^+, the higher desolvation barriers must be overcome from −0.65 eV to −3.83 eV. For example, the dissociation of Li $(DME)_4^+$ to Li $(DME)_3^+$ and the free DME molecule requires a desolvation energy of 36.84 kJ mol^{-1} (Fig. 3A). However, the SAFe/CVRCS helps to accelerate this process, and the spontaneous dissociation was achieved by changing the strong coordination structure of Li$(DME)_n^+$ to a weak coordination structure.

To visualize this process, the *in situ* sum frequency generation (SFG) method was developed to explore the dynamic desolvation evolution behavior at the interface (Fig. 3B). At the open-circuit voltage (OCV) state, distinct vibration peaks of C═O and C–H assigned to solvent molecules were observed.

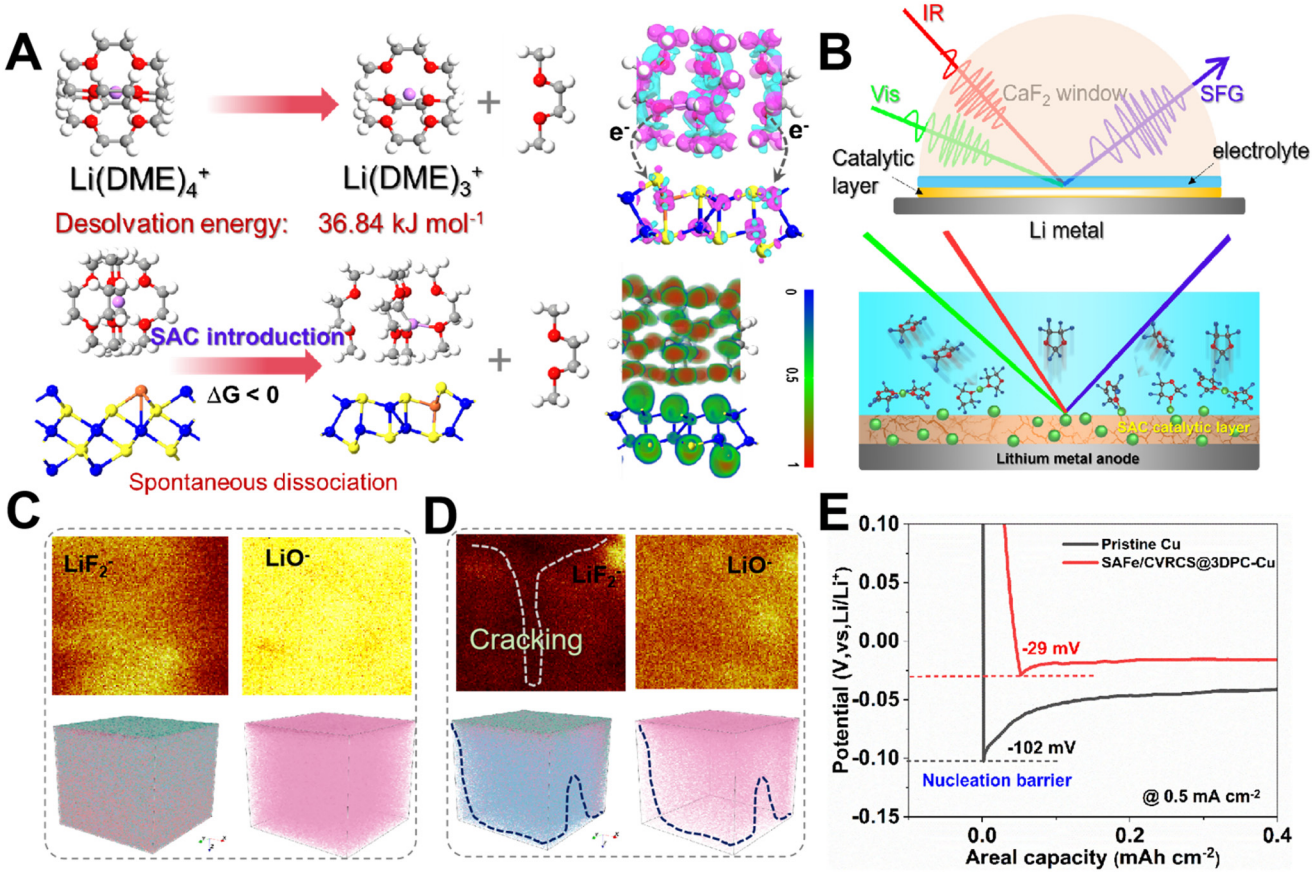

Fig. 3 (A) SAC accelerates Li $(DME)_n^+$ desolvation. (B) Characterization of SFG in monitoring interfacial desolvation. TOF-SIMS of (C) SAFe/CVRCS@3DPC-Li and (D) original Li. (E) Nucleation overpotential. Reproduced with permission.[50] Copyright 2023, Wiley-VCH.

Once a bias voltage is applied to the two systems, the characteristic peak intensity of the solvent at the interface decreases. However, the SAFe/CVRCS@3DPC-based system exhibited much lower intensity, indicating the superior capability of SAFe/CVRCS@3DPC in dissociating Li^+ from Li^+-solvent clusters. The dendrite growth and obvious cracks on the pristine Li anode were observed by applying an *ex situ* scanning electron microscope (SEM), which was also detected by time-of-flight secondary-ion mass spectrometry (TOF-SIMS). Simultaneously, LiF_2^- and LiO^- in the SAFe/CVRCS@3DPC-Li electrode were concentrated on the electrode surface and evenly distributed uniformly, which was mutually verified with the results of smooth metallic Li plating on the surface of SAFe/CVRCS@3DPC-Li electrode (Fig. 3C and D). Consequently, the SAFe/CVRCS@3DPC-Cu electrode had a lower nucleation barrier (29 mV), and the SAFe/CVRCS@3DPC-decorated symmetrical Li cell had a surprisingly long lifetime of 1600 h at 0.5 mA cm^{-2} (Fig. 3E). A high-capacity retention of 90.5% was achieved after 300 cycles at 0.5 C in the optimized Li-$LiFePO_4$ full cell. Under the catalytic effect of SAFe/CVRCS, solvated Li^+ was immediately dissociated at the interface of the catalytic layer, and then free Li^+ and solvent were generated at the interface, which accelerated the kinetics of Li^+ nucleation and smooth Li anode formation.

3.2 SACs in delocalizing lateral Li^+/Li^0 diffusion

SACs, with their highly active sites, can accelerate the desolvation process of lithium ions, releasing Li^+ from the solvation structure. Following desolvation, the uniformity of Li^+ distribution and diffusion is also responsible for the possible deposition of Li^0 against Li dendrites.[8,34,42] To deal with the potential barriers, inspired by the high catalytic activity of SACs, the atomic Zn on the MXene layer (Zn-MXene) shows that Li^+ can be nucleated uniformly on Zn-MXene and exhibits a smooth surface during the initial plating stage.[57] Through the synergistic interaction of a strong electric field at the edge of MXene and numerous Zn atoms, the nucleation barrier of Li^+ was reduced, and the deposition of Li^0 was rapidly promoted. Enhancing the areal capacity to 60 μA h cm^{-2}, the surface of Zn-MXene could afford bowl-like Li deposition without dendrites. In addition, a detailed understanding of Zn single-atom catalysts (ZnSAs) in Li metal batteries was investigated through theoretical calculation and chronoamperometry characterization. The physical properties of electronic density difference, binding bond, and Li^+ migration were compared with/without ZnSAs. Compared to graphene, significant delocalization was detected at the entire plane of the ZnSAs, indicating that the space electron redistribution is attributed to the atomic Zn (Fig. 4A).[58] More importantly, the lower binding energy of Li^0 on ZnSAs (−3.66 *vs.* −2.37 eV) indicates a higher probability of Li^+ deposition at the ZnSA site. Simultaneously, the surface migration energy barrier of Li^0 in ZnSAs is also the lowest, suggesting that Li^0 can easily migrate to adjacent regions, which contributes to the uniform deposition of Li^0 and that the ZnSA-modified Li anode exhibits lower plating/stripping overpotential (12 mV).

By regulating the core metal atom of SACs, electron density states are redistributed, thereby improving catalytic activity. The 3D structure of lithiophilic monatomic Co grew on N-doped carbon nanosheet-carbon fiber cloth (CC@CN-SACo) and was designed for dendrite-free Li metal batteries.[59] The Fermi level of the Co site shifts upon interaction with Li^0 adsorption, especially for the $3d_{z2}$ and $3d_{xz}$. More importantly, the Li-s orbital hybridized with the Co $3d_{z2}$ and $3d_{xz}$ orbitals forms a strong electron pairing, resulting in the high activity of the SACo site (Fig. 4B and C). It is worth mentioning that the SEI film generated on the CC@CN-SACo@Li anode was more stable, inhibiting the continuous occurrence of side reactions, and the symmetric cell maintained excellent long-term stability (500 h at 5 mA cm^{-2}). Inspired by sulfur cathode systems, the molecular dynamics (MD) simulation of single atom Fe as lithiophilic sites in an N-doped carbon matrix (Fe_{SA}–N–C) shows that Li^+ tends to diffuse around Fe_{SA}–N–C, rather than being randomly distributed on the original carbon substrate.[60] Meanwhile, the radial distribution function (RDF) in Fig. 4D showed that there was a weak characteristic peak between Li^+ and carbon structure (at 0.6–0.7 nm), while the peak between Li^+ and Fe_{SA}–N–C was sharp (at 0.2 nm), indicating the lithiophilicity of Fe_{SA}–N–C.

Various lithiophilic and catalytic activities of metal atoms have been screened and guided for experiments. Different single atoms were modeled on the N-doped graphene, and the corresponding adsorption energies of Li were calculated and compared. The interaction force between the metal atoms and the N atom promotes the charge transfer from the SAC sites to the graphene substrate, thereby optimizing the local electronic structure (Fig. 4E).[61] Moreover, the introduction of heteroatoms improves the lipophilicity and optimizes the nucleation behavior of Li^+. Among them, SAZr@NG had the largest Li^0 binding energy (−3.24 eV), while SAMn@NG had the lowest (−1.42 eV). However, the selection of SACs not only focuses on the single theoretical value of adsorption energy, but the stability of the SAC structure is also very important. Fig. 4F shows that with the increase in plating amount, the bond length and angle of SAZr@NG changed dramatically (~0.103 Å, ~9.05°), leading to the collapse of the structure and the decrease in catalytic activity. On the contrary, the structural change in SAMn@NG was much smaller than in other control groups (~0.005 Å, ~0.06°). Although much progress has been achieved in the regulation of SACs, the research on optimizing and reducing the nucleation energy barriers is still in its infancy and early stage.

In addition to the central sites, the structures of the SACs also include the adjacent coordination atoms and the functional hosts. Notably, the regulation of coordination atoms also causes local charge redistribution and a change in charge transfer paths (Fig. 5A). To identify the catalytic nature from the regulation of coordination atoms and coordination bonds, Zhai *et al.* constructed single atom loaded N-doped graphene (SAM-NG) to form an M–N_x–C nanostructure, exploring the relationships between SAC structure and catalytic activity.[62] Fig. 5B depicts the randomness of the Li^+ nucleation site on the bare carbon substrate, while the lithiophilic metal hetero-

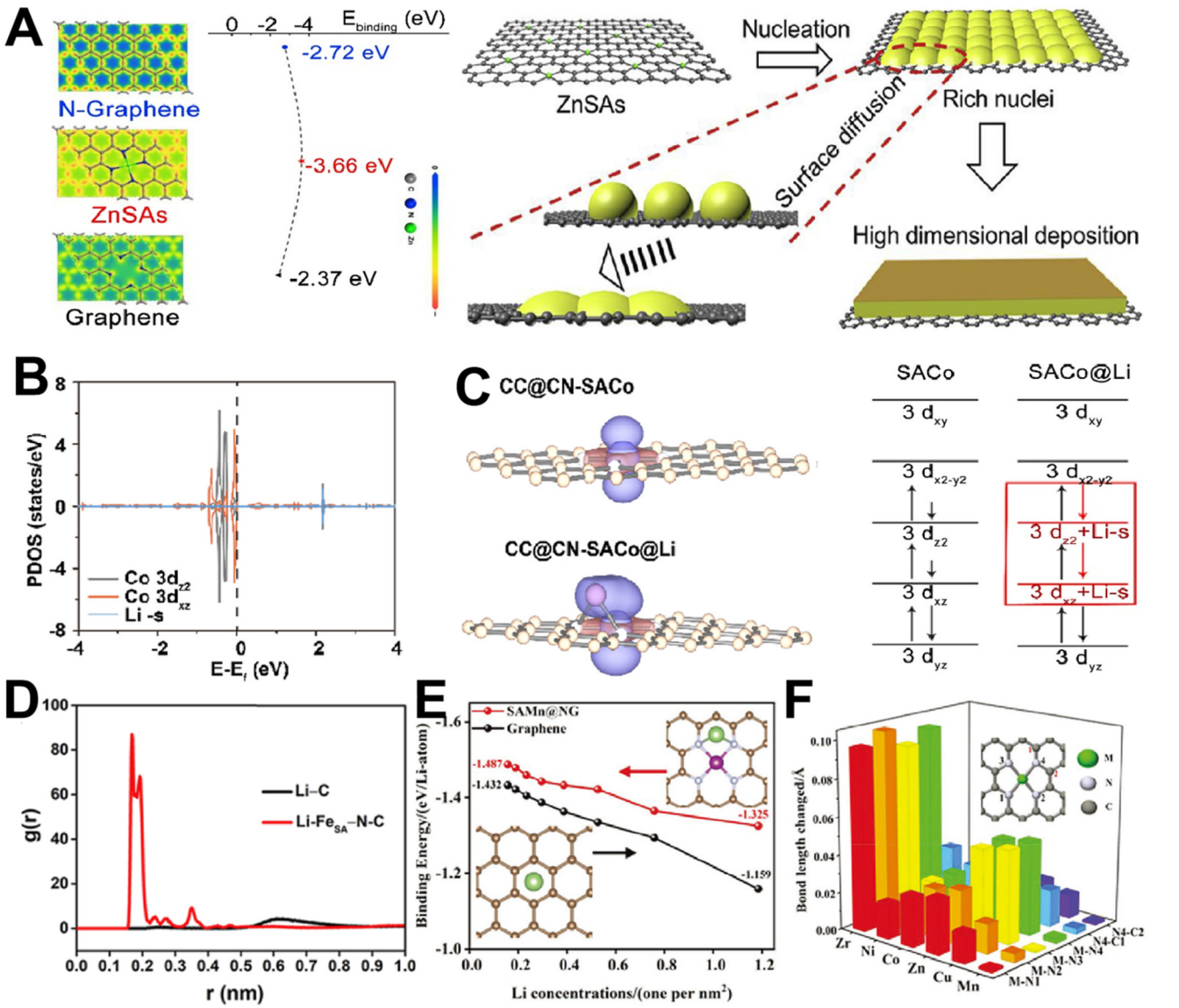

Fig. 4 (A) Comparisons of electron density difference and surface binding energy. Reproduced with permission.[58] Copyright 2019, Elsevier. (B) PDOS. (C) Orbital changes in Co atoms before and after adsorption of Li. Reproduced with permission.[59] Copyright 2023, Elsevier. (D) Diagram of Fe_{SA}–N–C reducing Li^+ nucleation overpotential and RDFs. Reproduced with permission.[60] Copyright 2019, American Chemical Society. (E) Theoretical simulation of Li binding energy and structure stability. (F) Binding energy diagram of Li^0 at different SAM@NGs and (G) relative change in the bond length.[61] Reproduced with permission. Copyright 2022, Wiley-VCH.

atoms regulate the nucleation barrier of Li^+ and promote the uniform deposition of Li^0. In this case, the single-atom Ni on the NG (SANi-NG)-based electrode had a smooth surface at 0.5 mA h cm^{-2} (10 h), while the pristine graphene sample had a bumpy surface (Fig. 5C). Besides, single atom Ni onto 3D ordered mesoporous N-doped carbon was constructed, and related coordination atoms affecting the charge transport and electron cloud distribution in the active site were also revealed. Despite the nitrogen-related coordination environment, different chemical coordinations for constructing an asymmetric SAC environment are considered to achieve high catalytic activity. For example, asymmetric N- and O-coordinating Co atoms (Co–N/O) on graphene were proposed to accelerate the deposition kinetics of Li^+. As shown in Fig. 5D, the co1 site in the Co–N/O-500 had the largest Li^+ binding energy (−1.832 eV), and the adsorption capacity of the coordination atom N was also improved to a certain extent (N1 site, from −0.751 eV to −0.963 eV).[63] In addition, the free energy of Li^+ to Li^0 showed that the asymmetric coordination environment of O and N increased the active site activity of the Co and reduced the nucleation barrier of Li^+ (Fig. 5E).[64] Therefore, the asymmetric coordination environment can induce the charge rearrangement of the central atom so that the catalytic activity of Co, N, and O atoms can be jointly improved.

Optimizing the structure of SAC can improve the catalytic ability, and the number of active sites further increases the

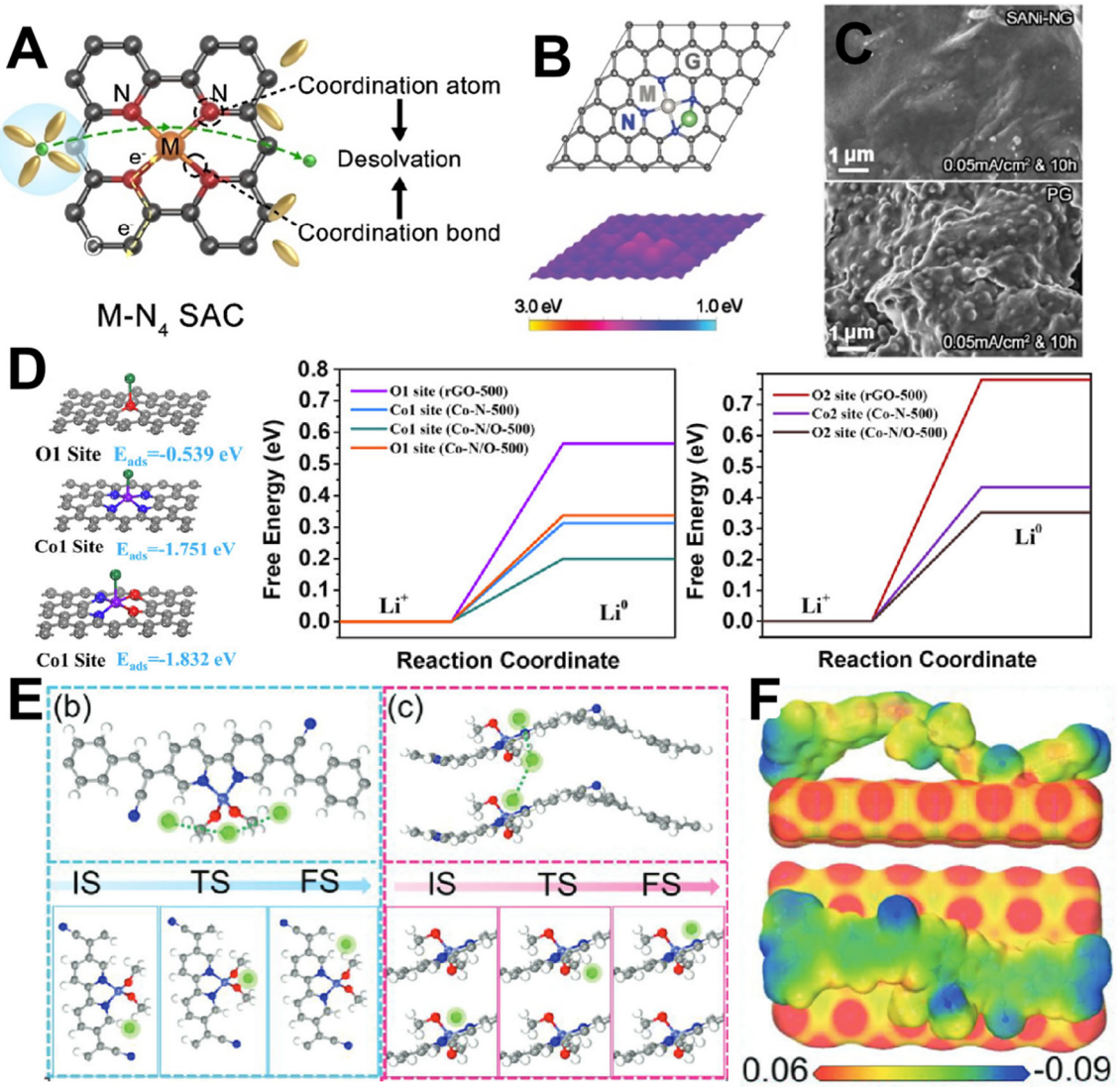

Fig. 5 (A) Schematic of coordination atoms and coordination bonds of SAC on Li^+ desolvation and reduction of the Li^+ nucleation barrier. Schematic of Li nucleation and the plating process on (B) the SAM-NG electrode. (C) SEM images of the different electrodes. Reproduced with permission.[62] Copyright 2019, Wiley-VCH. (D) Adsorption structures and the corresponding adsorption energies of Co–N/O toward Li^+. Reproduced with permission.[63] Copyright 2023, Wiley-VCH. (E) Free energy of the conversion of Li^+ to Li^0 on Co–N/O. (F) Schematic diagram of Li^+ transmission in sp^2c-COF-Co and the corresponding energy barrier. Reproduced with permission.[64] Copyright 2023, Wiley-VCH.

catalytic efficiency. The nucleation and plating behaviors of metallic Li are closely related to the number of active sites. Compared with inorganic carbon substrate materials, the 2D conjugated organic covalent organic framework (COF) has more functional groups and can provide more abundant active sites. Zhang and co-workers optimized the local coordination environment by trapping a single atom Co in a coordination conjugate COF (sp^2c-COF-Co).[64] The DFT calculation results show that the Co–N coordination and cyano-group (strong electron absorption) induced the electron transfer from the Co site to the bipyridine site and then constructed a local electron-rich state, which also accelerated the migration of Li^+ and inhibited the dendrites growth (Fig. 5F). The theoretical calculation further verifies that the SACo made the binding force of Li^+ with sp^2c-COF-Co better than that of sp^2c-COF (−3.302 *vs.* −1.856 eV). Based on this, suitable lithiophilicity, appropriate porosity and charge transfer induced by SACo promote the high migration barrier (0.532 eV) of Li^+ in the sp^2c-COF-Co plane direction. Therefore, the sp^2c-COF-based cell had a high Li^+ transfer number (0.76) and a very low Li^+ nucleation barrier (8 mV).

In our previous studies on sulfur cathode catalysts, the defect-rich metal oxides/sulfides can change the electron density, thereby accelerating the conversion kinetics of polysulfides.[42,54,65,66] This inspired us to determine whether SACs can be introduced on nanoparticles to further enhance the catalytic efficiency. The methodology of "SAC-in-Defects", which utilizes the abundant defect sites in semiconducting

nanocrystals to capture SACs, has been proposed and successfully implemented.[8] The active single atom Co on defective iron sulfide and layered porous carbon (SACo/ADFS@HPSC) acted as the validation model. Catalyzed and guided by highly active SACo, much lower Li^+ nucleation from 18 to 12.5 mV was achieved, and the cycle life of the SACo/ADFS@HPSC-modified Li electrode was extended to 1600 h (Fig. 6A). Meanwhile, the cycled surface morphologies of the original Li electrode and SACo/ADFS@HPSC-Li show that SACo/ADFS@HPSC regulates the distribution of Li^+ flux and inhibits dendrite growth (Fig. 6B and C). On this basis, the large number of atomic Co active sites in SACo/ADFS@HPSC is beneficial for accelerating Li^+ transport and averaging related Li^+ spatial distribution. The uniformly deposited Li^0 prefers to deposit along the Li surface, thereby inhibiting dendrite growth. Impressively, the fabrication of a pouch cell based on SACo/ADFS@HPSC-Li with sulfur loading up to 5.4 mg cm^{-2} could provide an outstanding area capacity of 3.78 mA h cm^{-2}, Which can provide full energy for smart devices.

To explore catalytic activity at the heterojunction interface, atomic Pt into In_2S_3/Ti_3C_2 binary nanosheets (Pt SAs/In_2S_3/Ti_3C_2) was designed to protect Li anode.[67] The rearrangement of electron density at the interface of Pt SAs/In_2S_3 and Ti_3C_2 contributed to the exchange of the electrons from Li^+ to Li^0, which significantly reduced the nucleation barrier of Li^+ and inhibited the formation of Li dendrites (Fig. 6D). Thus, the Pt SAs/In_2S_3/Ti_3C_2@PP-based symmetrical cell had a very low overpotential (~49.6 mV) even after 1100 h plating/stripping at 1 mA cm^{-2}. Furthermore, the Pt SAs/In_2S_3/Ti_3C_2 separator modification simultaneously fulfilled the functions of inhibiting polysulfides with the shuttle effect. Under sulfur loading (6.4 mg cm^{-2}), the Pt SAs/In_2S_3/Ti_3C_2-based Li–S cells exhibited an excellent long cycle life.

As discussed above, the single-metal atom catalyst could reduce the barriers of desolvation, ion migration, and diffusion at the interface and promote the nucleation of Li^+ to Li^0. However, the deposition behavior of Li^0 was also known to be influenced by the interfacial tension, and the surface diffusion is limited by a high barrier. More importantly, compared with the original Li surface, the Li^0 binding energy was increased from 1.388 to 1.589 and 1.611 eV after introducing SAFe and SANi, respectively.[34] Moreover, the diffusion energy barriers of Li^0 at SAFe@NC and SANi@NC were further reduced, enabling smooth transverse surface diffusion of Li^0

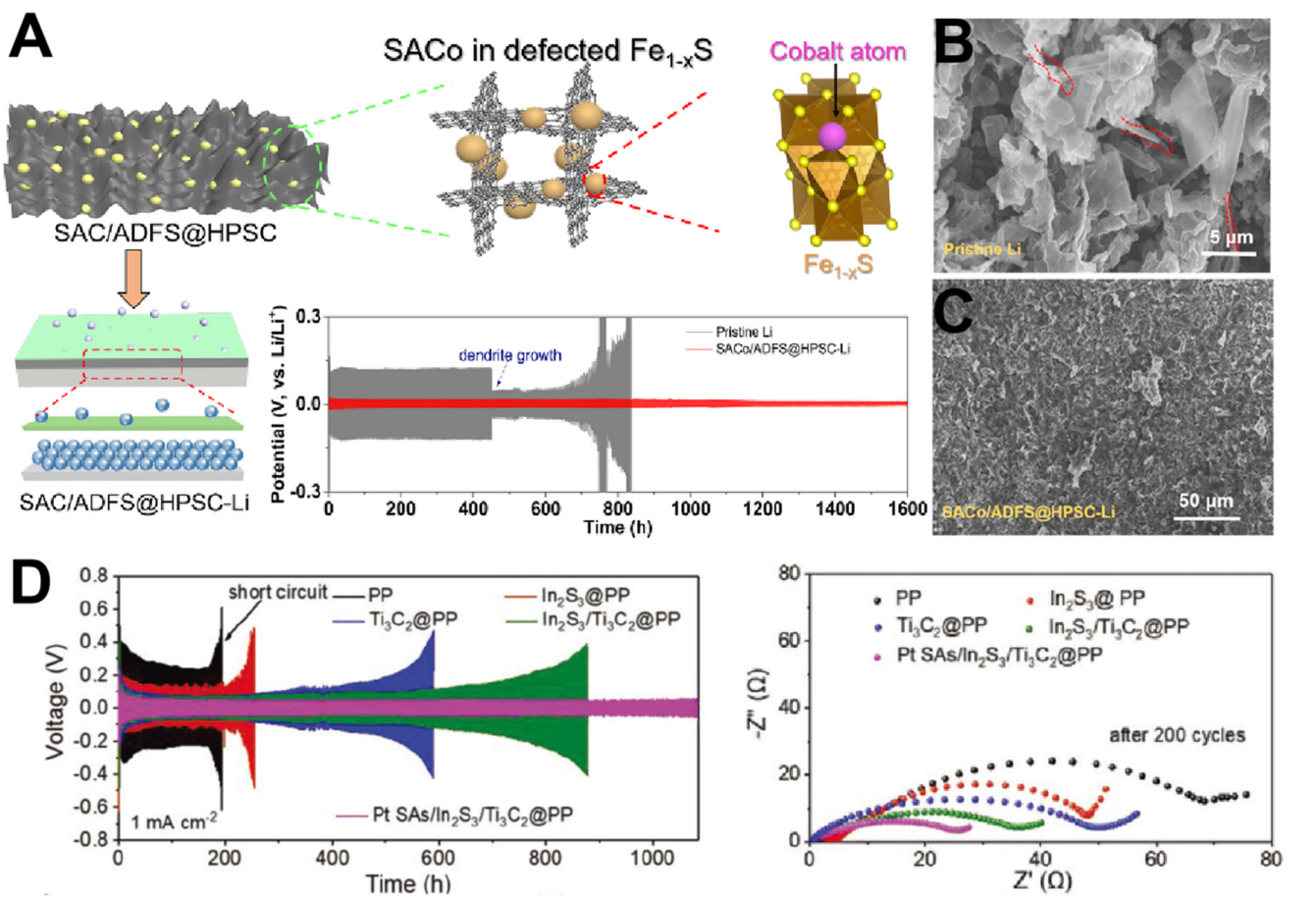

Fig. 6 (A) SEM images of the different electrodes after plating. (B) Schematic of plated metallic Li behaviors on Li without/with SACo/ADFS@HPSC. (C) Soft pack battery application. Reproduced with permission.[8] Copyright 2021, American Chemical Society. (D) Voltage–time curves of different separator modifications based on Li//Li symmetric cells. Reproduced with permission.[67] Copyright 2022, Wiley-VCH.

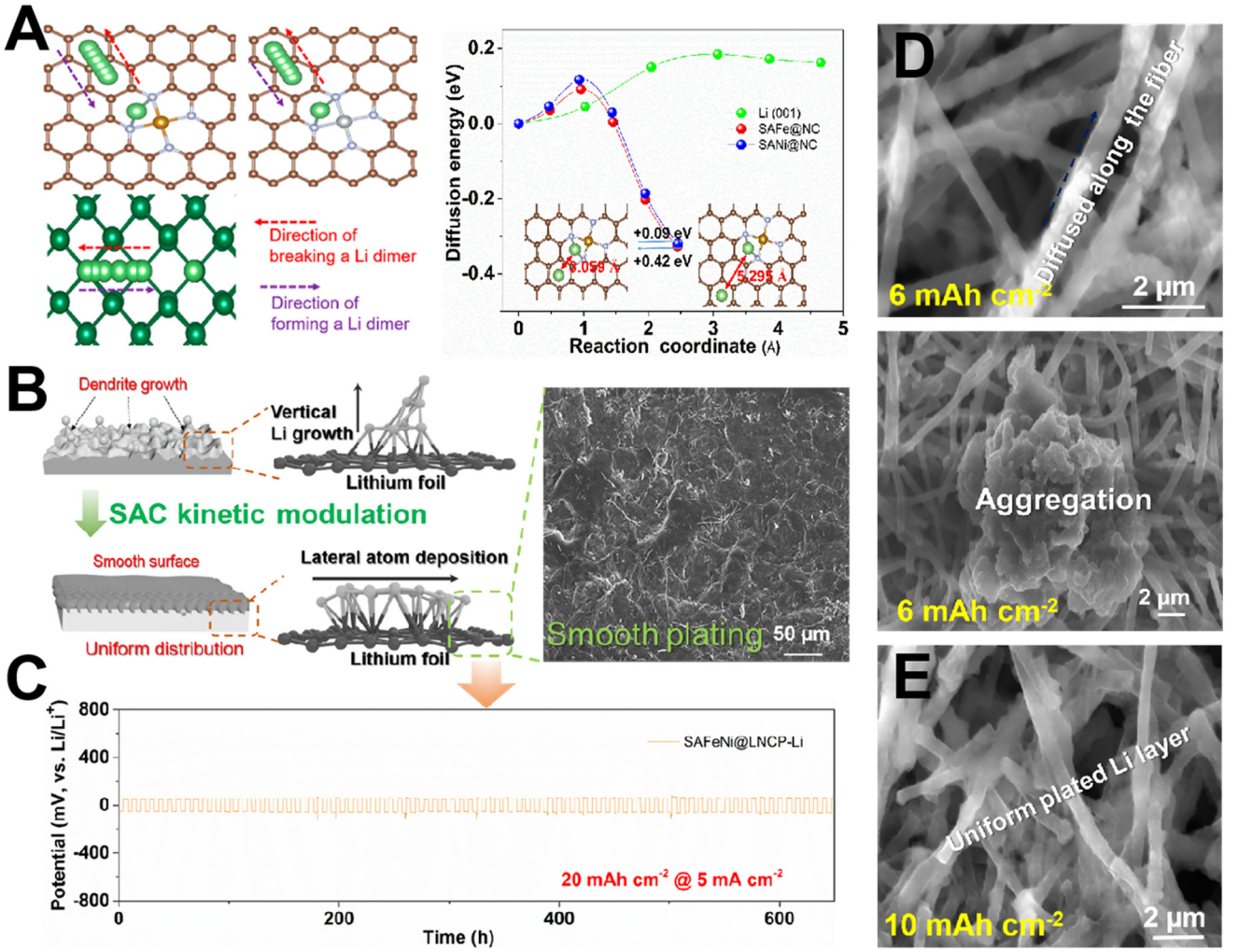

Fig. 7 (A) Simulated diffusion barriers of Li^0 on different theoretical models. (B) Schematic diagram of SAC promoting uniform diffusion of Li^0 at the interface. (C) Symmetric cell at 5 mA cm^{-2} under 20 mA h cm^{-2}. SEM images of (D) the LNCP and (E) LNCP electrode surfaces after plating. Reproduced with permission.[34] Copyright 2022, American Chemical Society.

(Fig. 7A). To signify the catalytic efficiency, the binary Ni and Fe metal atoms in ultralight N-doped carbon nanofiber paper (SAFeNi@LNCP) were proposed. The SEM images in Fig. 7B further verify that Li^0 was uniformly deposited and transversely diffused across the surface of SAFeNi@LNCP under the synergistic action of SAFe and SANi, while the deposition of Li^0 on the bare LNCP substrate showed serious aggregation (Fig. 7D and E). Consequently, the SAFeNi@LNCP-Li-based cell had a lower overpotential (25 mV) and a longer plating/stripping life (900 h) at the practical capacity of 3 mA h cm^{-2}, showing great prospects for future applications (Fig. 7C). Therefore, the deposition behavior of Li^0 was influenced by the current density and the Li^0 diffusion rate. When the deposition rate of Li^0 exceeds the diffusion rate with increasing current, Li^0 grows vertically on the surface of Li metal, and then dendrites are generated. After the introduction of SACs, the diffusion rate of Li^0 at the active site was accelerated to achieve the uniform diffusion and lateral redistribution of Li^0 on the anode surface. Therefore, the SAFeNi@LNCP-Li-based cell had a lower overpotential (25 mV) and longer plating/stripping life (900 h) at the practical capacity of 3 mA h cm^{-2}, showing great promise for future applications.

4. Single atom catalysts in alkali metal batteries beyond lithium

Furthermore, concerns over the geographical availability and cost of lithium metal have recently triggered the study and development of a "post-lithium" battery technology based on more naturally abundant alkali elements, such as Na. Owing to the abundance of elemental Na in nature, Na metal anode has received more attention in industrial and research fields. Similar to metallic Li, metallic Na anode also suffers from dendrite formation and "dead Na" during the continuous plating/stripping process, which in turn poses a safety risk to bat-

teries.[68] Similar to Li anode, Li *et al.* adopted functional hollow carbon nanotubes with single atom Zn embedded in a carbon shell (Zn_{SA}-HCNT) as a promotor of Na^+ plating/stripping kinetics.[69] The *In situ* TEM in Fig. 8A shows that the metallic Na grew uniformly along the tube wall of Zn_{SA}-HCNT until it was completely coated, and the diameter of the tube wall increased from the original 330 to 410 nm during plating and gradually decreased to 340 nm during the subsequent stripping process, indicating that the Zn_{SA}-HCNT had sufficient strength and the ability to promote the rapid transport of Na^+, reduce the nucleation barrier of Na^+ and inhibit the growth of Na dendrites.[69] The Na symmetrical cell based on Zn_{SA}-HCNT electrodes can achieve a long cycle life of over 900 h at a high current density of 10 mA cm^{-2}. The anode substrate plays an important role in the nucleation behavior and deposition kinetics of metal ions. The carbon substrate with N anchored single atom Zn on carbon substrates (ZnSA–N–C) was used to match the nucleation and deposition kinetics of

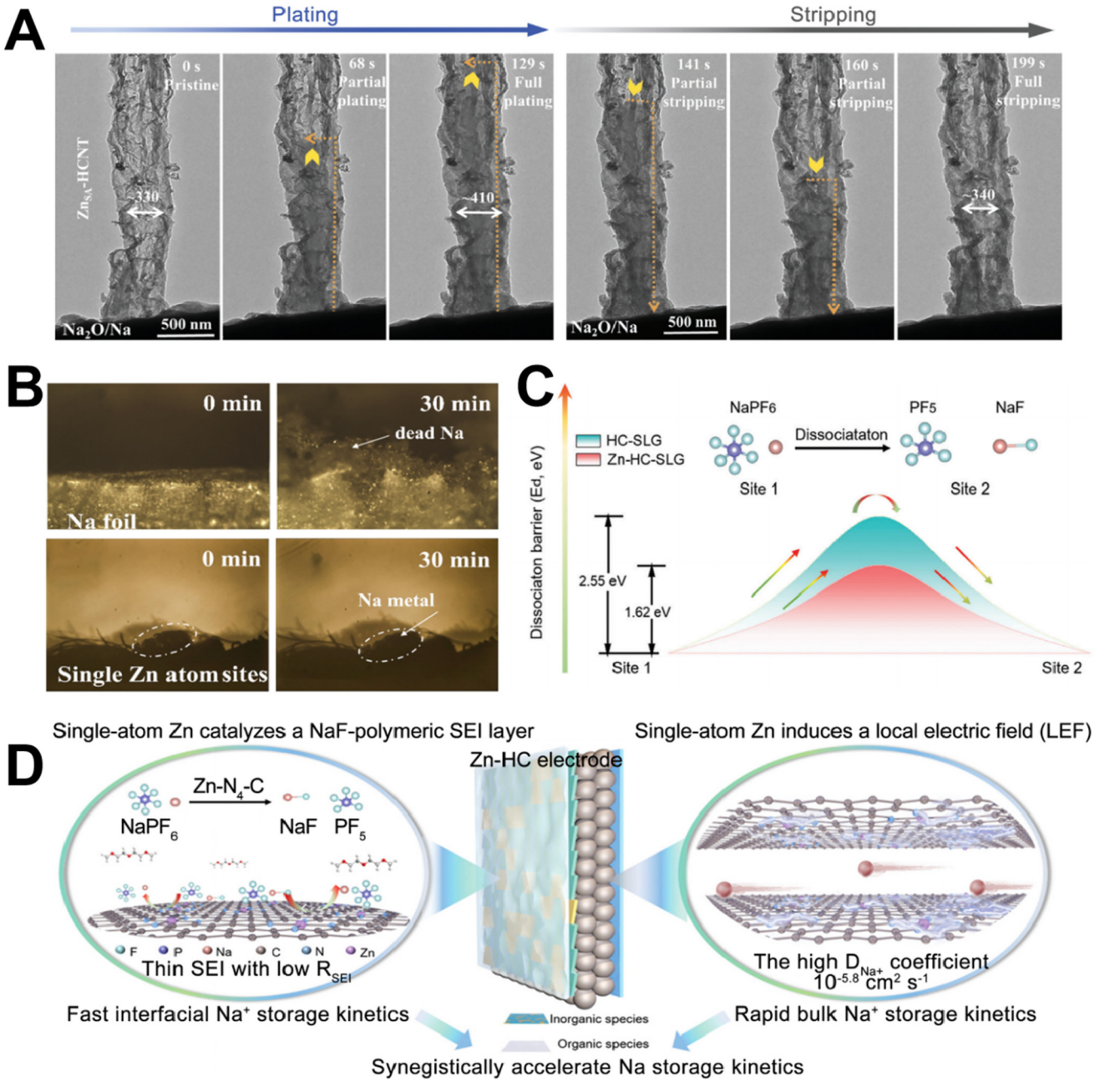

Fig. 8 (A) *In situ* TEM observation of metallic Na plating/stripping on the ZnSA-HCNT anode.[69] Copyright 2022, Wiley-VCH. (B) *In situ* optical microscopy observations. Reproduced with permission.[70] Copyright 2019, American Chemical Society. (C) Dissociation energy barrier of HC-SLG with/without SAZn to catalyze $NaPF_6$. (D) Schematic of the Zn-HC-enhanced rate capability mechanism. Reproduced with permission.[71] Copyright 2023, Wiley-VCH.

Na^+ to achieve the protection of the Na anode. The results show that Na^+ on ZnSA–N–C had a very low nucleation overpotential (0 mV), which is much lower than that on carbon cloth (9 mV) and bare copper foil (32 mV) substrates. In particular, SAZn had a strong binding ability for Na^+ (0.34 eV *vs.* 0.09 eV), which can act as a sodiophilic site to achieve rapid nucleation and uniform diffusion of metallic Na. Simultaneously, the *in situ* optical microscopy results showed that dendrites and dead sodium quickly appeared on the bare copper foil within 30 min of plating (Fig. 8B).[70] However, homogeneous metallic Na deposition occurs on the surface of the ZnSA–N–C-based electrode, which preferentially nucleates at the SAZn site. Thus, the Na–Zn_{SA}–N–C-based symmetrical cell had a long plating/stripping life of 1000 h at 0.5 mA cm^{-2}.

It should be noted that the solvation phenomenon of Na^+ with a delayed solvation shell structure becomes more severe as the ambient temperature is lowered, leading to a decrease in ion mobility in the bulk or at the interface. As discussed in the Li metal anode, it is of great interest to accelerate the sluggish diffusion/transport kinetics of Na^+ at low temperatures using catalytic SACs. The placement of single-atom Zn on hard carbon (Zn-HC) on metallic Na and the long cycle life at low temperatures was demonstrated by Lu *et al.*[71] Meanwhile, the DFT results in Fig. 8C revealed that the modulated electronic site of Zn-HC promoted the decomposition of $NaPF_6$ and the formation of Na–F (1.62 *vs.* 2.55 eV), contributing to the formation of a dense and uniform NaF-dominated SEI layer. The results of F 1s of Zn–HC after SEI formation showed that the content of the Na–F characteristic peak (25.4%) was higher than that of HC (12.1%), proving that SAZn accelerated the decomposition of $NaPF_6$. Simultaneously, the establishment of a local electric field promoted the adsorption, transport, and storage of Na^+ at the interface, achieving excellent cycling stability at −40 °C (85% capacity retention after 400 cycles, Fig. 8D).[71]

To improve the utilization of metallic Na, a porous N-doped carbon with a single atom Co (Co_{SA}@NC) was prepared by direct pyrolysis of Co-doped organometallic frameworks.[72] The images of the morphology evolution of metallic Na plating during the cycling were recorded using SEM and cryo-transmission electron microscope (Cryo-TEM) techniques. It can be observed that the rod-shaped Na dendrite was initially generated on the Co nanoparticle-controlled electrode and that the generated dendrite shape changed to a nubby-like with some "dead Na". In Cryo-TEM, the Co_{SA}@NC matrix showed a lateral uniform distribution of plated Na on the surface and dead Na-free morphology, which can be ascribed to the numerous well-distributed catalytic Co_{SA} sites in the direction of Na migration. As simulated by theoretical calculation, the Co_{SA} sites also exhibit a strong affinity to Na^0 (−2.29 eV), further smoothing the deposition of Na^+. The nucleation barrier was extremely reduced with the highest activity of single atom Co sites for Na^+ plating (11.5 mV overpotential, at 0.5 mA cm^{-2}). Increasing the binding strength between the active site and the carbon substrate can promote the stability of the structure, thereby achieving the long-term cycling stability of the battery at 0.5 C (473 mA h g^{-1} after 500 cycles).

As another sustainable energy storage technology, potassium metal batteries have also shown potential for application in large-scale energy storage due to their low cost, abundant resources, and suitable working potential.[73] Compared with Li^+ and Na^+, K^+ has a smaller solvation radius (4.8 Å *vs.* 4.6 Å *vs.* 3.6 Å), a faster ion diffusion rate, and a lower solvation energy barrier. However, consistent with Li and Na, slow nucleation kinetics and uncontrollable dendrite formation have also limited the development of potassium metal batteries at the laboratory stage. As mentioned above, SACs could accelerate the desolvation of alkali metal ions and reduce the nuclear barrier, thereby promoting the uniform diffusion of metal atoms. The biocarbon substrate modified by a single-atomic Co catalyst (SA-Co@HC) was used as a host for K metal to achieve a dendrite-free K metal battery.[74] Furthermore, the porous and vertical channels in HC can provide pathways and space for metallic K deposition. Simultaneously, SA-Co had a better K^0 adsorption energy (−1.16 eV) to reduce the nucleation barrier of K^+. Therefore, the overpotential (3 mV) of the SA-Co@HC electrode was much smaller than that of the Cu foil and HC electrodes. More importantly, the uneven deposition of metallic K in the bare Cu foil during the long cycle induced the uneven distribution of the electric field, which in turn generates dendrites and continuously destroys SEI. The simulation results and SEM images showed that there was a more direct and efficient K^+ transport route in the SA-Co@HC/K composite electrode, and the current was evenly distributed, resulting in the long-cycle stability of the K metal battery (over 2500 h). These results clearly demonstrated the potential of SACs in boosting the Na and K metal battery technologies. However, their development is still at a very preliminary research level.

5. Sustainable path for future critical battery chemistry and technology

5.1 Sustainable materials for next-generation battery chemistry

It has been demonstrated that SACs can be utilized to enhance battery performance, particularly in Li-based batteries, allowing for kinetic and uniform plating. To achieve sustainability in battery chemistry, it is essential to consider the necessary factors, such as cost, availability of elemental resources, and life-time cycling assessment.[75,76] These crucial variables play a major role in the development of next-generation battery chemistry. As is known, the practical applications of batteries are significantly determined by the cost and energy density of the electrode materials.[77] The abundance of elements used in batteries intrinsically determines their cost. Currently, there is a shift in focus from lithium-based batteries to other post-lithium ion/metal batteries, whose elements are more abundant on the earth and more sustainable (Fig. 9). This shift has spurred the development of next-generation alkaline ion batteries, such as sodium and potassium-based batteries or high volumetric-energy magnesium/calcium batteries.[78,79]

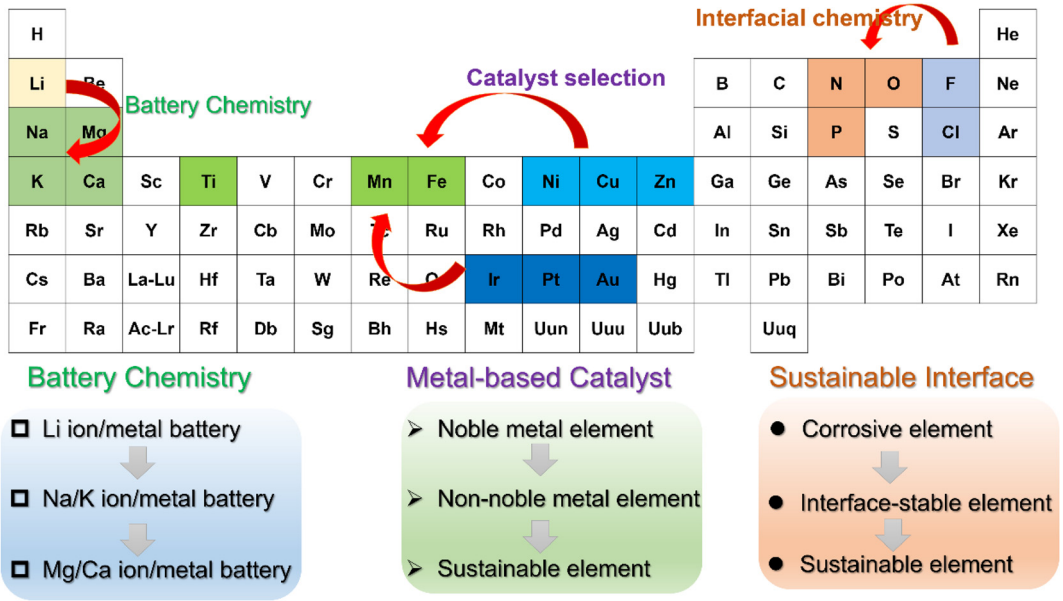

Fig. 9 Sustainable path and material selection for future critical battery chemistry based on SACs.

In addition to the direct transition of alkali metal, several challenges still remain in the electrode materials, especially on the cathode side, which strongly relies on the transition metals. Efforts should also be devoted to reducing the cost and environmental impact of electrode materials. For example, the organic electrode materials are proposed as "green" and sustainable alternatives to conventional inorganic compounds.[80,81] Beyond conventional insertion cathodes, the exploitation of O_2 or CO_2 as cathodes in alkali metal batteries enables a much higher theoretical energy density integrating battery sustainability, in which the energy storage chemistries for cathode and anode get a potential breakthrough by the SAC chemistry.[82,83] In terms of electrochemical catalysts, various metal-based elements, ranging from noble to non-noble metals, are being utilized or studied as indicated in above works. The primary concern is that elemental abundance and sustainability determine the same standard for choosing metal atoms, even though they may have compromised electrochemical activity or efficiency. For example, cobalt-based catalysts are currently regarded as the most efficient catalysts, and they are much more expensive than iron-based catalysts. However, the exposure of cobalt is believed to severely threaten environmental harmony by contaminating the soil and water and introducing health risks, such as neurotoxicity.[84] Despite the electrode materials, the electrolyte chemistry is also very crucial for greener, safer, and more sustainable batteries. The widely used organic electrolyte systems in current batteries need to be considered by replacing green components, such as F-free solvents and salts, even though the cathode or anode contains less rare or toxic metal.[85] Because of the presence of F-related ingredients in some electrolytes, such as PF_6^- or FEC, these F-containing electrolyte additives or salts may break down and experience side reactions under certain cycles at the electrolyte/electrode interface, which inevitably generate corrosive byproducts, toxic gas or substance and cause uneven SEI on the electrode surface. To help achieve a sustainable and green electrolyte, further intense focus or attention is required in selecting green salts, solvents and electrolyte additives. With significant effort, aqueous battery systems or novel green chemistry for designing sustainable battery materials may offer a sustainable path toward a greener future.[86–88] Therefore, the integration of SACs in alkali metal batteries is a multifaceted approach that addresses several aspects of sustainability, from material selection to environmental impact, and can significantly advance the field of green energy storage.

5.2 Greener synthesis of atomic catalysts for sustainable battery technologies

Because of the 100% exposure, the SACs have an extremely active catalytic capacity. As described in section 2, high-temperature pyrolysis and wet immersion chemistry are the two current methods used to synthesize SACs.[89] The methodology described above unavoidably involves the use of some organic solvents or energy-consuming processes, neither of which is advantageous for advancing the sustainability of scale-up production. Generally, synthesis variables, such as the presence of the center metal atom, the ability to adsorb materials, and the chemical structures, are linked to the catalytic activity and efficiency.[90] Green chemistry requires redesigning or optimizing the fabrication process to avoid using dangerous chemicals or solvents.[90] Different coordination environments, such as heteroatoms and defects, can be controlled to load SACs at high concentrations without aggregating. Using a distinct coupling mechanism that exhibits gradual activity, the precise modulation of a metal atom from one atom to multiple atoms can be achieved. Furthermore, the broader electronic inter-

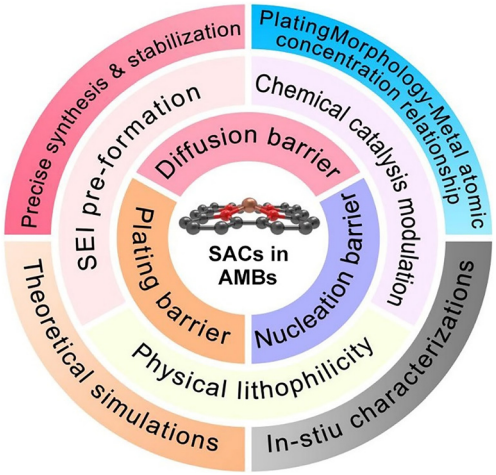

Fig. 10 Challenges and prospective summary of single atom catalyst modulators in alkali metal batteries.

action surrounding metal atoms and metal-based compound hosts may also be used to anchor single metal atoms, demonstrating the interconnected charge transfer across the interface.[91] The optimal catalysts presented in the study should maintain their activity and catalytic efficiency from nanoscale to meter scale during the process of scaling up production. A new path to different types of metal atoms may also be made possible by intensifying efforts to streamline the template-assistance synthesis procedure.[34,42] In addition to the aforementioned interfacial "single-atom-in-defects" catalysts, other methods for preparing SACs have also been explored, such as electrochemical methods and the molten salt method, which represent milder, more environment-friendly and energy-efficient routes towards high-quality SACs.[92,93] Apart from atomic metal designs, creative schemes and additional support are crucial factors that impact commercialization to achieve the goals of "Carbon-Peak" and "Carbon-Neutralization". Better yet, the atomic metals show varying catalytic capacities due to distinct elemental coordination sites. To advance the sustainability narrative in the fields of green energy and green chemistry, particularly in relation to SACs for battery technologies, it is essential to innovate by enhancing the structural architecture of catalysts, optimizing the interaction at coordination sites, and conducting more extensive environmental impact assessments. This holistic strategy aims to maximize efficiency and minimize the ecological footprint in the development and application of next-generation energy storage technologies.

6. Conclusion and prospects

In summary, the applications of SACs in alkali–metal anodes has opened a new route for fabricating dendrite-free alkali metal batteries. SACs on the hybrid matrix provide the high ability to break down associated barriers to modulate the kinetics of interfacial desolvation, ion diffusion and atomic diffusion. Resorting to the uniform distribution of active SACs, a uniform alkali metal deposition layer can be easily achieved by the delocalization of atoms with random dendrite growth disappearance activity. Despite several advances achieved, the development of using SACs on metallic alkali metal surfaces is still in its infancy, and further attempts should be made, as suggested in the following aspects (Fig. 10):

(1) *Scale-up fabrication with high atomic loading of SACs*: as discussed above, the ability to manipulate surfaces is influenced by catalytic site numbers or concentrations. Improving the catalytic atom concentration in the modulation layer would be beneficial for achieving a smoother lithium layer. To date, the fabrication of SACs is mainly supported on heteroatom-doped nanocarbon or defective metal materials and lacks technical capabilities for scale-up. Developing theoretical calculations for screening highly efficient SACs for alkali metal anode is required prior to synthesis. A new methodology should be developed to synthesize SACs with large-scale output. Meanwhile, conducting a systematic summary or comparison is recommended to further guide the synthesis directions.

(2) *Quantitative assessment between catalytic efficiency and plating morphology*: as stated in previous reports, the electronic density distribution of edged metal atoms in the matrix affects the plating morphology. As illustrated, it is proposed to develop precise interfacial analysis and quantitative detection methods to study exploration. For example, more reliable and rapid detection methods to accurately identify the type, position, and concentration of SACs are urgently required prior to interfacial analysis. For a better understanding of the catalytic or modulating ability of alkali metal batteries, standard comparison parameters or processes should be established to evaluate the practical effects of lowering energy barriers. For example, the practical stripping/plating capacity of 3 mA h cm^{-2} at a standard current density of 3 mA cm^{-2} should be set when comparing the cycling lifespan or coulombic efficiency. It is also recommended to calculate the total gram capacity of the alkali metal electrode, including all materials on the anode side.

(3) *Recognizing ion/atom transport pathway across the SAC-decorated artificial layer*: many reports in the literature have demonstrated that fabricating an electron-conductive artificial layer with SACs on the top surface of lithium metal foil, the lithium plating process still occurs mainly on the bottom lithium foil instead of depositing on the upper surface of conductive layers. Considering that the lithium ions can already be reduced electrochemically when they reach the electron-conductive layer, one has to admit that the lithium atoms created in this way will migrate to the lithium foil rather than be deposited immediately on the local place of the artificial layer according to the experimental results. However, the key role of such conductive artificial layers with SACs is still ambiguous in achieving dendrite-free and smooth lithium plating. It appears that a clearer representation of the atomic diffusion diagram can help modulate the lateral diffusion rate to achieve dendrite-free plating more effectively. Moreover, it is suggested to demonstrate whether the same phenomena occur in other alkali metal systems.

(4) *Extending SACs to decorated high conductive modulator/electrolyte*: owing to the functionality of SACs in lowering desolvation barriers and ion/atom diffusion across/along the surface, it is meaningful to observe whether the SACs could change Li^+ solvation shell structure when immersed in electrolytes. Furthermore, to deal with the problem of ion transport in solid-state electrolytes, one could try whether the SACs play a similar role in solid-state alkali metal batteries to accelerate the diffusion of metal ions at the electrolyte–electrode interface. Further experiments are urgently needed to expand the application of SACs in alkali metal batteries.

(5) *Adopting in situ/operando characterizations to trace plating evolution and mechanism*: to date, little attention and few useful *in situ* characterizations have focused on the post-lithium metal battery field.[94–96] Most researchers apply optical instruments to observe the smooth plating tenability of the alkali metal from a macro-view for comparison. However, the valid detailed information to disclose the interfacial interaction between alkali metal atoms and SACs is still missing, and a non-destructive, precise, *in situ*, and real-time detection method is more and more urgently required to uncover the underlying mechanisms. For example, *in situ* XAS could help determine the bond environment between SACs and atoms. By combining EELS with cryo-TEM, real-time interaction videos and electronic/chemical structure development can be created.

Data availability

Data availability does not apply to this article because no new data were created or analyzed in this review.

Conflicts of interest

There are no conflicts to declare.

Acknowledgements

Dr Jian Wang acknowledges the Fellowship supported by the Alexander von Humboldt Foundation. This work is also funded by the National Key R&D Program of China (2021YFA1201503), Natural Science Foundation of Jiangsu Province (No. BK20210130), the China Postdoctoral Science Foundation (2023M730885, 2023M732561), and the National Natural Science Foundation of China (No. 22279161, 22309144, 52307236). The authors also thank the technical support from Nano-X, Suzhou Institute of Nano-tech and Nano-bionics, Chinese Academy of Sciences.

References

1 J. W. Choi and D. Aurbach, *Nat. Rev. Mater.*, 2016, **1**, 1–16.
2 J. Wang, L. Jia, H. Lin and Y. Zhang, *ChemSusChem*, 2020, **13**, 3404–3411.
3 J. Wang, L. Li, H. Hu, H. Hu, Q. Guan, M. Huang, L. Jia, H. Adenusi, K. V. Tian, J. Zhang, S. Passerini and H. Lin, *ACS Nano*, 2022, **16**, 17729–17760.
4 J. Zhang, R. He, L. Jia, C. You, Y. Zhang, M. Liu, N. Tian, H. Lin and J. Wang, *Adv. Funct. Mater.*, 2023, **33**, 2305674.
5 J. M. Zheng, M. H. Engelhard, D. H. Mei, S. H. Jiao, B. J. Polzin, J. G. Zhang and W. Xu, *Nat. Energy*, 2017, **2**, 17012.
6 Y. Liu, Q. Liu, L. Xin, Y. Liu, F. Yang, E. A. Stach and J. Xie, *Nat. Energy*, 2017, **2**, 17083.
7 J. Zhang, Y. Su and Y. Zhang, *Nanoscale*, 2020, **12**, 15528–15559.
8 J. Wang, J. Zhang, S. Cheng, J. Yang, Y. Xi, X. Hou, Q. Xiao and H. Lin, *Nano Lett.*, 2021, **21**, 3245–3253.
9 B. Liu, J.-G. Zhang and W. Xu, *Joule*, 2018, **2**, 833–845.
10 L. Xu, S. Tang, Y. Cheng, K. Wang, J. Liang, C. Liu, Y.-C. Cao, F. Wei and L. Mai, *Joule*, 2018, **2**, 1991–2015.
11 S. Li, L. Fan and Y. Lu, *Energy Storage Mater.*, 2019, **18**, 205–212.
12 J. Wang, J. Yang, Q. Xiao, J. Zhang, T. Li, L. Jia, Z. Wang, S. Cheng, L. Li, M. Liu, H. Liu, H. Lin and Y. Zhang, *Adv. Funct. Mater.*, 2020, **31**, 2007434.
13 S. Huang, L. Chen, T. Wang, J. Hu, Q. Zhang, H. Zhang, C. Nan and L. Z. Fan, *Nano Lett.*, 2021, **21**, 791–797.
14 L. Li, M. Wang, J. Wang, F. Ye, S. Wang, Y. Xu, J. Liu, G. Xu, Y. Zhang, Y. Zhang, C. Yan, N. V. Medhekar, M. Liu and Y. Zhang, *J. Mater. Chem. A*, 2020, **8**, 8033–8040.
15 G. Zhou, S. Zhao, T. Wang, S. Z. Yang, B. Johannessen, H. Chen, C. Liu, Y. Ye, Y. Wu, Y. Peng, C. Liu, S. P. Jiang, Q. Zhang and Y. Cui, *Nano Lett.*, 2020, **20**, 1252–1261.
16 J. Wang, H. Hu, S. Duan, Q. Xiao, J. Zhang, H. Liu, Q. Kang, L. Jia, J. Yang, W. Xu, H. Fei, S. Cheng, L. Li, M. Liu, H. Lin and Y. Zhang, *Adv. Funct. Mater.*, 2021, **32**, 2110468.
17 T. Chen, J. Liu, D. Losic, J. Wang and H. Zhang, *ChemSusChem*, 2023, e202301242, DOI: **10.1002/cssc.202301242**.
18 Q. Kang, Z. C. Zhuang, Y. Li, Y. Z. Zuo, J. Wang, Y. J. Liu, C. Q. Shi, J. Chen, H. F. Li, P. K. Jiang and X. Y. Huang, *Nano Res.*, 2023, **16**, 9240–9249.
19 Q. Kang, Z. Zhuang, Y. Liu, Z. Liu, Y. Li, B. Sun, F. Pei, H. Zhu, H. Li, P. Li, Y. Lin, K. Shi, Y. Zhu, J. Chen, C. Shi, Y. Zhao, P. Jiang, Y. Xia, D. Wang and X. Huang, *Adv. Mater.*, 2023, **35**, e2303460.
20 Q. Kang, Y. Li, Z. Zhuang, H. Yang, L. Luo, J. Xu, J. Wang, Q. Guan, H. Zhu, Y. Zuo, D. Wang, F. Pei, L. Ma, J. Zhao, P. Li, Y. Lin, Y. Liu, K. Shi, H. Li, Y. Zhu, J. Chen, F. Liu, G. Wu, J. Yang, P. Jiang and X. Huang, *Adv. Mater.*, 2024, **36**, 2308799.
21 L. Jia, H. Hu, X. Cheng, H. Dong, H. Li, Y. Zhang, H. Zhang, X. Zhao, C. Li, J. Zhang, H. Lin and J. Wang, *Adv. Energy Mater.*, 2023, **14**, 2304010.
22 X.-Q. Zhang, X.-B. Cheng, X. Chen, C. Yan and Q. Zhang, *Adv. Funct. Mater.*, 2017, **27**, 1605989.
23 S. Liu, G. R. Li and X. P. Gao, *ACS Appl. Mater. Interfaces*, 2016, **8**, 7783–7789.

24 S. Choudhury and L. A. Archer, *Adv. Electron. Mater.*, 2016, **2**, 1500246.
25 J. Wang, J. Yang, Q. Xiao, L. Jia, H. Lin and Y. Zhang, *ACS Appl. Mater. Interfaces*, 2019, **11**, 30500–30507.
26 X. B. Cheng, H. J. Peng, J. Q. Huang, R. Zhang, C. Z. Zhao and Q. Zhang, *ACS Nano*, 2015, **9**, 6373–6382.
27 B. Zhu, Y. Jin, X. Hu, Q. Zheng, S. Zhang, Q. Wang and J. Zhu, *Adv. Mater.*, 2017, **29**, 1603755.
28 Y. Zhang, C. Wang, G. Pastel, Y. Kuang, H. Xie, Y. Li, B. Liu, W. Luo, C. Chen and L. Hu, *Adv. Energy Mater.*, 2018, **8**, 1800635.
29 M. Zhu, B. Li, S. Li, Z. Du, Y. Gong and S. Yang, *Adv. Energy Mater.*, 2018, **8**, 1703505.
30 L. Ye, M. Liao, H. Sun, Y. Yang, C. Tang, Y. Zhao, L. Wang, Y. Xu, L. Zhang, B. Wang, F. Xu, X. Sun, Y. Zhang, H. Dai, P. G. Bruce and H. Peng, *Angew. Chem., Int. Ed.*, 2019, **58**, 2437–2442.
31 H. Ye, Z. J. Zheng, H. R. Yao, S. C. Liu, T. T. Zuo, X. W. Wu, Y. X. Yin, N. W. Li, J. J. Gu, F. F. Cao and Y. G. Guo, *Angew. Chem., Int. Ed.*, 2019, **58**, 1094–1099.
32 C. Yang, Y. Yao, S. He, H. Xie, E. Hitz and L. Hu, *Adv. Mater.*, 2017, **29**, 1702714.
33 J. Wang, H. Hu, J. Zhang, L. Li, L. Jia, Q. Guan, H. Hu, H. Liu, Y. Jia, Q. Zhuang, S. Cheng, M. Huang and H. Lin, *Energy Storage Mater.*, 2022, **52**, 210–219.
34 J. Wang, J. Zhang, S. Duan, L. Jia, Q. Xiao, H. Liu, H. Hu, S. Cheng, Z. Zhang, L. Li, W. Duan, Y. Zhang and H. Lin, *Nano Lett.*, 2022, **22**, 8008–8017.
35 J. Cui, S. Yao, M. Ihsan-Ul-Haq, J. Wu and J.-K. Kim, *Adv. Energy Mater.*, 2019, **9**, 1802777.
36 X. R. Chen, Y. X. Yao, C. Yan, R. Zhang, X. B. Cheng and Q. Zhang, *Angew. Chem., Int. Ed.*, 2020, **59**, 7743–7747.
37 P. Biswal, S. Stalin, A. Kludze, S. Choudhury and L. A. Archer, *Nano Lett.*, 2019, **19**, 8191–8200.
38 X. F. Yang, A. Wang, B. Qiao, J. Li, J. Liu and T. Zhang, *Acc. Chem. Res.*, 2013, **46**, 1740–1748.
39 H. Zhang, G. Liu, L. Shi and J. Ye, *Adv. Energy Mater.*, 2017, **8**, 1701343.
40 J. Wang, L. Jia, J. Zhong, Q. Xiao, C. Wang, K. Zang, H. Liu, H. Zheng, J. Luo, J. Yang, H. Fan, W. Duan, Y. Wu, H. Lin and Y. Zhang, *Energy Storage Mater.*, 2019, **18**, 246–252.
41 J. Wang, L. Jia, S. Duan, H. Liu, Q. Xiao, T. Li, H. Fan, K. Feng, J. Yang, Q. Wang, M. Liu, J. Zhong, W. Duan, H. Lin and Y. Zhang, *Energy Storage Mater.*, 2020, **28**, 375–382.
42 J. Zhang, C. You, H. Lin and J. Wang, *Energy Environ. Mater.*, 2022, **5**, 731–750.
43 P. Song, M. Luo, X. Liu, W. Xing, W. Xu, Z. Jiang and L. Gu, *Adv. Funct. Mater.*, 2017, **27**, 1700802.
44 Y. Chen, S. Ji, Y. Wang, J. Dong, W. Chen, Z. Li, R. Shen, L. Zheng, Z. Zhuang, D. Wang and Y. Li, *Angew. Chem., Int. Ed.*, 2017, **56**, 6937–6941.
45 P. Yin, T. Yao, Y. Wu, L. Zheng, Y. Lin, W. Liu, H. Ju, J. Zhu, X. Hong, Z. Deng, G. Zhou, S. Wei and Y. Li, *Angew. Chem., Int. Ed.*, 2016, **55**, 10800–10805.
46 K. Jiang, S. Siahrostami, A. J. Akey, Y. Li, Z. Lu, J. Lattimer, Y. Hu, C. Stokes, M. Gangishetty, G. Chen, Y. Zhou, W. Hill, W.-B. Cai, D. Bell, K. Chan, J. K. Nørskov, Y. Cui and H. Wang, *Chem*, 2017, **3**, 950–960.
47 Z. Du, X. Chen, W. Hu, C. Chuang, S. Xie, A. Hu, W. Yan, X. Kong, X. Wu, H. Ji and L. J. Wan, *J. Am. Chem. Soc.*, 2019, **141**, 3977–3985.
48 M. M. Millet, G. Algara-Siller, S. Wrabetz, A. Mazheika, F. Girgsdies, D. Teschner, F. Seitz, A. Tarasov, S. V. Levchenko, R. Schlogl and E. Frei, *J. Am. Chem. Soc.*, 2019, **141**, 2451–2461.
49 Y. Chen, S. Ji, C. Chen, Q. Peng, D. Wang and Y. Li, *Joule*, 2018, **2**, 1242–1264.
50 J. Wang, J. Zhang, J. Wu, M. Huang, L. Jia, L. Li, Y. Zhang, H. Hu, F. Liu, Q. Guan, M. Liu, H. Adenusi, H. Lin and S. Passerini, *Adv. Mater.*, 2023, **35**, e2302828.
51 J. Wan, W. Chen, C. Jia, L. Zheng, J. Dong, X. Zheng, Y. Wang, W. Yan, C. Chen, Q. Peng, D. Wang and Y. Li, *Adv. Mater.*, 2018, **30**, 1705369.
52 A. Zitolo, V. Goellner, V. Armel, M. T. Sougrati, T. Mineva, L. Stievano, E. Fonda and F. Jaouen, *Nat. Mater.*, 2015, **14**, 937–942.
53 Q. Guan, J. Wang, Q. Zhuang, J. Zhang, L. Li, L. Jia, Y. Zhang, H. Hu, H. Hu, S. Cheng, H. Zhang, H. Li, M. Liu, S. Wang and H. Lin, *Energy Environ. Sci.*, 2024, **17**, 3765–3775.
54 J. Zhang, R. He, Q. Zhuang, X. Ma, C. You, Q. Hao, L. Li, S. Cheng, L. Lei, B. Deng, X. Li, H. Lin and J. Wang, *Adv. Sci.*, 2022, **9**, e2202244.
55 Z. Zhang, J. Wang, H. Qin, B. Zhang, H. Lin, W. Zheng, D. Wang, X. Ji and X. Ou, *ACS Nano*, 2024, **18**, 2250–2260.
56 Z. Wu, Y. Zuo, Y. Zhang, X. Li, J. Zhang, Y. Wang, C. Shen, X. Cheng, M. Liu, H. Liu, H. Lin, J. Wang, L. Zhan and L. Ling, *Energy Storage Mater.*, 2024, **70**, 103463.
57 J. Gu, Q. Zhu, Y. Shi, H. Chen, D. Zhang, Z. Du and S. Yang, *ACS Nano*, 2020, **14**, 891–898.
58 K. Xu, M. Zhu, X. Wu, J. Liang, Y. Liu, T. Zhang, Y. Zhu and Y. Qian, *Energy Storage Mater.*, 2019, **23**, 587–593.
59 Z. Liang, C. Peng, J. Shen, Y. Yang, S. Yao, D. Xue, M. Zhu and J. Liu, *J. Power Sources*, 2023, **556**, 232474.
60 Y. Sun, J. Zhou, H. Ji, J. Liu, T. Qian and C. Yan, *ACS Appl. Mater. Interfaces*, 2019, **11**, 32008–32014.
61 Z. Yang, Y. Dang, P. Zhai, Y. Wei, Q. Chen, J. Zuo, X. Gu, Y. Yao, X. Wang, F. Zhao, J. Wang, S. Yang, P. Tang and Y. Gong, *Adv. Energy Mater.*, 2022, **12**, 2103368.
62 P. Zhai, T. Wang, W. Yang, S. Cui, P. Zhang, A. Nie, Q. Zhang and Y. Gong, *Adv. Energy Mater.*, 2019, **9**, 1804019.
63 Y. Li, D. Fang, X. L. Li, D. Yan, S. Xi, T. C. Li, C. Lin, S. Huang, J. Qiu, X. Xu and H. Y. Yang, *Energy Environ. Mater.*, 2023, **6**, e12449.
64 C. Zhang, J. Xie, C. Zhao, Y. Yang, Q. An, Z. Mei, Q. Xu, Y. Ding, G. Zhao and H. Guo, *Adv. Mater.*, 2023, **35**, e2304511.
65 J. Wang, L. Jia, H. Liu, C. Wang, J. Zhong, Q. Xiao, J. Yang, S. Duan, K. Feng, N. Liu, W. Duan, H. Lin and Y. Zhang, *ACS Appl. Mater. Interfaces*, 2020, **12**, 12727–12735.

66 S. Cheng, J. Wang, S. Duan, J. Zhang, Q. Wang, Y. Zhang, L. Li, H. Liu, Q. Xiao and H. Lin, *Chem. Eng. J.*, 2021, **417**, 128172.
67 C. Zhou, M. Li, N. Hu, J. Yang, H. Li, J. Yan, P. Lei, Y. Zhuang and S. Guo, *Adv. Funct. Mater.*, 2022, **32**, 2204635.
68 H. Li, H. Zhang, F. Wu, M. Zarrabeitia, D. Geiger, U. Kaiser, A. Varzi and S. Passerini, *Adv. Energy Mater.*, 2022, **12**, 2202293.
69 X. Li, W. Ye, P. Xu, H. Huang, J. Fan, R. Yuan, M. S. Zheng, M. S. Wang and Q. Dong, *Adv. Mater.*, 2022, **34**, e2202898.
70 T. Yang, T. Qian, Y. Sun, J. Zhong, F. Rosei and C. Yan, *Nano Lett.*, 2019, **19**, 7827–7835.
71 Z. Lu, J. Wang, W. Feng, X. Yin, X. Feng, S. Zhao, C. Li, R. Wang, Q. A. Huang and Y. Zhao, *Adv. Mater.*, 2023, **35**, e2211461.
72 Y. Li, P. Xu, J. Mou, S. Xue, S. Huang, J. Hu, Q. Dong, C. Yang and M. Liu, *Small Methods*, 2021, **5**, e2100833.
73 P. Liu and D. Mitlin, *Acc. Chem. Res.*, 2020, **53**, 1161–1175.
74 D. Zhang, X. Ma, L. Wu, J. Wen, F. Li, J. Zhou, A. M. Rao and B. Lu, *Adv. Energy Mater.*, 2022, **13**, 2203277.
75 C. P. Grey and J. M. Tarascon, *Nat. Mater.*, 2016, **16**, 45–56.
76 Z. Yang, H. Huang and F. Lin, *Adv. Energy Mater.*, 2022, **12**, 2200383.
77 A. Innocenti, S. Beringer and S. Passerini, *Nat. Rev. Mater.*, 2024, **9**, 347–357.
78 G. N. Newton, L. R. Johnson, D. A. Walsh, B. J. Hwang and H. Han, *ACS Sustainable Chem. Eng.*, 2021, **9**, 6507–6509.
79 P. Xu, D. H. S. Tan and Z. Chen, *Trends Chem.*, 2021, **3**, 620–630.
80 Z. Song and H. Zhou, *Energy Environ. Sci.*, 2013, **6**, 2280–2301.
81 J. Hu, Y. Hong, M. Guo, Y. Hu, W. Tang, S. Xu, S. Jia, B. Wei, S. Liu, C. Fan and Q. Zhang, *Energy Storage Mater.*, 2023, **56**, 267–299.
82 Z. Lian, Y. Lu, C. Wang, X. Zhu, S. Ma, Z. Li, Q. Liu and S. Zang, *Adv. Sci.*, 2021, **8**, 2102550.
83 E. Zhang, A. Dong, K. Yin, C. Ye, Y. Zhou, C. Tan, M. Li, X. Zheng, Y. Wang, X. Gao, H. Li, D. Wang and S. Guo, *J. Am. Chem. Soc.*, 2024, **146**, 2339–2344.
84 L. Leyssens, B. Vinck, C. Van Der Straeten, F. Wuyts and L. Maes, *Toxicology*, 2017, **387**, 43–56.
85 H. Chen, M. Armand, M. Courty, M. Jiang, C. P. Grey, F. Dolhem, J. M. Tarascon and P. Poizot, *J. Am. Chem. Soc.*, 2009, **131**, 8984–8988.
86 A. Innocenti, D. Bresser, J. Garche and S. Passerini, *Nat. Commun.*, 2024, **15**, 4068.
87 J. Wang, H. Hu, L. Jia, J. Zhang, Q. Zhuang, L. Li, Y. Zhang, D. Wang, Q. Guan, H. Hu, M. Liu, L. Zhan, H. Adenusi, S. Passerini and H. Lin, *InfoMat*, 2024, **6**, e12558.
88 H. Li, Z. Chen, L. Zheng, J. Wang, H. Adenusi, S. Passerini and H. Zhang, *Small Methods*, 2023, **8**, 2300554.
89 J. Wang, J. Zhang, Y. Zhang, H. Li, P. Chen, C. You, M. Liu, H. Lin and S. Passerini, *Adv. Mater.*, 2024, **36**, 2402792.
90 S. Mitchell, R. Qin, N. Zheng and J. Perez-Ramirez, *Nat. Nanotechnol.*, 2021, **16**, 129–139.
91 P. Chen, T. Wang, D. He, T. Shi, M. Chen, K. Fang, H. Lin, J. Wang, C. Wang and H. Pang, *Angew. Chem., Int. Ed.*, 2023, **62**, e202311693.
92 D. Lin, T. Wang, Z. Zhao, Y. Liu, H. Song, X. Yang, Z. Li, S. Yao, X. Hu, L. Lei, B. Yang and Y. Hou, *Nano Energy*, 2023, **113**, 108568.
93 J. Luo, G. I. N. Waterhouse, L. Peng and Q. Chen, *Ind. Chem. Mater.*, 2023, **1**, 486–500.
94 T. A. Wynn, J. Z. Lee, A. Banerjee and Y. S. Meng, *MRS Bull.*, 2018, **43**, 768–774.
95 G. Rong, X. Zhang, W. Zhao, Y. Qiu, M. Liu, F. Ye, Y. Xu, J. Chen, Y. Hou, W. Li, W. Duan and Y. Zhang, *Adv. Mater.*, 2017, **29**, 1606187.
96 J. Wang, H. Liu, J. Zhang, Q. Xiao, C. Wang, Y. Zhang, M. Liu, Q. Kang, L. Jia, D. Wang, Q. Li, W. Duan, H. Adenusi, S. Passerini, Y. Zhang and H. Lin, *Energy Storage Mater.*, 2024, **67**, 103289.